Geophysical Research Letters

RESEARCH LETTER
10.1029/2023GL105583

Dry Air Outbreak and Significant Surface Turbulent Heat Loss During Hurricane Ian: Satellite and Saildrone Observations

Lisan Yu[1], Yanxu Chen[1], Alex O. Gonzalez[1], Chidong Zhang[2], and Gregory R. Foltz[3]

[1]Department of Physical Oceanography, Woods Hole Oceanographic Institution, Woods Hole, MA, USA, [2]Pacific Marine Environmental Laboratory, NOAA, Seattle, WA, USA, [3]Atlantic Oceanographic and Meteorological Laboratory, NOAA, Miami, FL, USA

Key Points:

- Hurricane Ian triggered a dry air outbreak, causing substantial turbulent heat loss (>850 Wm^{-2}) and Gulf of Mexico surface cooling (~1.4°C)
- Winds, not air-sea humidity, are a dominant contributor to turbulent heat flux in the tropical Atlantic warm water pool
- Saildrone's high-frequency linewise data, differing from satellite's footprint averages, offer unique insight into high wind variability

Supporting Information:

Supporting Information may be found in the online version of this article.

Correspondence to:

L. Yu,
lyu@whoi.edu

Citation:

Yu, L., Chen, Y., Gonzalez, A. O., Zhang, C., & Foltz, G. R. (2023). Dry air outbreak and significant surface turbulent heat loss during Hurricane Ian: Satellite and saildrone observations. *Geophysical Research Letters*, *50*, e2023GL105583. https://doi.org/10.1029/2023GL105583

Received 9 AUG 2023
Accepted 27 NOV 2023

Author Contributions:

Conceptualization: Lisan Yu
Data curation: Lisan Yu, Chidong Zhang, Gregory R. Foltz
Formal analysis: Lisan Yu
Funding acquisition: Lisan Yu
Investigation: Lisan Yu
Methodology: Lisan Yu
Project Administration: Lisan Yu
Software: Lisan Yu
Validation: Lisan Yu, Yanxu Chen, Alex O. Gonzalez, Chidong Zhang, Gregory R. Foltz
Visualization: Lisan Yu, Yanxu Chen
Writing – original draft: Lisan Yu

Abstract This study investigates an exceptional Gulf of Mexico dry air outbreak triggered by Hurricane Ian and fueled by dry air originating from drought-stricken mid-latitudes under a high-pressure system. The convergence of meteorological forces, combining cooler, dry air with a warmer, humid sea surface and strong winds, intensified latent and sensible heat exchanges, resulting in significant oceanic heat loss. Data from the 2022 Atlantic hurricane Saildrone mission and satellite flux analysis revealed that the outbreak's total turbulent heat fluxes peaked above 850 Wm^{-2}, comparable to or even surpassing the hurricane's impact. Argo float measurements recorded a 40-m deepening of the mixed layer and a 1.4°C temperature decrease. In the tropical Atlantic, wind effects outweighed humidity in driving flux variability. Saildrone's high-frequency linewise measurements, distinct from satellite's footprint averages, provide unique insights into wind variability under high wind conditions.

Plain Language Summary Dry air outbreaks in the Gulf of Mexico are meteorological events marked by the influx of drier and often cooler air masses into the typically warm and humid Gulf region. These events occur mostly during the fall and winter months and are associated with atmospheric circulation patterns, particularly the transit of high-pressure systems from the North American continent. This study highlights an exceptional dry air outbreak in late September 2022, triggered by Hurricane Ian and intensified by dry air originating from drought-stricken mid-latitudes, a condition sustained by a persistent high-pressure system. The interaction between cold, dry air and warm, humid sea surface, coupled with strong winds, intensified the turbulent transfer of heat from the ocean to the atmosphere, resulting in significant ocean heat loss. Data from the 2022 Atlantic hurricane Saildrone mission and satellite flux analysis revealed that the outbreak's total turbulent heat fluxes peaked above 850 Wm^{-2}, comparable to or even surpassing the hurricane's impact. Concurrently, the ocean's surface layer deepened by about 40 m, and the temperature dropped by around 1.4°C. These findings hold substantial implications for understanding the Gulf's weather patterns and their impact on tropical storms, with the potential to influence both their intensity and trajectories.

1. Introduction

Hurricane Ian, a formidable Category 5 system on the Saffir-Simpson Hurricane Wind Scale, made landfall in southwestern Florida on 28 September 2022, before veering northeastward and striking Georgetown, South Carolina, just 2 days later (Bucci et al., 2023). The impact of Ian's storm surge, accompanied by destructive winds gusting up to 72 m s^{-1} (140 knots) during its initial landfall, and excessive rainfall exceeding 15 inches, resulted in widespread inland flooding along its path.

Concurrently, on the northwestern flank of Hurricane Ian, a high-pressure system was developing over the Great Lakes region, while a persistent trough hovered over the eastern United States (Figure S1 in Supporting Information S1). The interaction between Ian's low-pressure system and the mid-latitude high pressure to its northwest, although less discussed, had equally significant ramifications. The intense pressure gradients between these meteorological phenomena gave rise to strong northeasterly winds, driving a surge of colder Canadian dry air along the storm's western periphery. The dry northeasterly winds swept through the eastern and central states, exacerbating already widespread severe droughts in those regions (Figure S2 in Supporting Information S1). The impacts were not limited to the mainland U.S.; as the high-pressure system advanced eastward across the Northeast during 28–30 September 2022 (Figure S1 in Supporting Information S1), the northeasterly winds

Writing – review & editing: Lisan Yu, Alex O. Gonzalez, Chidong Zhang, Gregory R. Foltz

pushed the dry air toward the sea, affecting both the Gulf of Mexico (GOM) and the coastal waters of the U.S. Atlantic.

Previous studies have shown that the impacts of dry air outbreaks over a moisture-laden sea surface bear resemblance to cold-air outbreaks occurring at mid-high latitudes (Nagano & Ando, 2020; Tilinina et al., 2018; Yoneyama & Parsons, 1999). Often accompanied by strong winds, these events increase the instability within the marine boundary layer and intensify the turbulent transfer of latent and sensible heat from the ocean to the atmosphere. Such dynamic interaction leads to significant heat loss from the ocean, inducing a cooling effect on the sea surface (Villanueva et al., 2010; Zavala-Hidalgo et al., 2014). A comparable atmosphere-ocean interaction was observed during the dry air outbreak amid Hurricane Ian, as indicated by satellite-based surface flux analysis. In situ evidence supporting these satellite observations was collected from uncrewed saildrones deployed as part of the hurricane saildrone mission (Foltz et al., 2022; Zhang et al., 2023) in the vicinity during that period.

This study has two main objectives. First, it aims to document the significant turbulent heat loss event associated with the dry air outbreak during Hurricane Ian, and the resulting surface cooling in the GOM. Second, it seeks to demonstrate the enhanced synergistic potential of satellite flux analysis and saildrone line-wise measurements, enabling a more comprehensive understanding of the spatial and dynamic aspects of air-sea interaction in the hurricane-prone region of the GOM and the western tropical Atlantic.

2. Data

The saildrone measurements used in the study were obtained during the 2022 Saildrone Hurricane Mission (Foltz et al., 2022; Zhang et al., 2023), conducted from mid-July to early November 2022 (Figures 1a–1c). This period typically corresponds to the Atlantic warm pool SST reaching its seasonal maximum, exceeding 28.5°C in the GOM, Caribbean Sea, and western tropical North Atlantic, aligning with the peak of tropical cyclone activities (Wang et al., 2008). The saildrone measurements represent 1-min averages sampled at 5-min intervals along the saildrone's path.

The surface turbulent latent heat flux (Q_{LH}), sensible heat flux (Q_{SH}), and momentum fluxes (wind stress ($\vec{\tau}$)), and flux-related surface meteorology are derived from the second generation Objectively Analyzed air-sea Fluxes (referred to as OAFlux2) (Yu & Weller, 2007). These fluxes are calculated from the Coupled Ocean-Atmosphere Response Experiment version 3.6 (COARE 3.6) algorithm (Fairall et al., 2003). OAFlux2 is produced daily at a 0.25° resolution. A 3-hr evaluation window was selected for saildrone-OAFlux2 comparisons. In addition, Argo data collected from 10th September to 20th October 2022 was used in assessing the subsurface temperature/salinity (T/S) variability in response to the significant surface heat loss. Readers are referred to Supporting Information S1 for a detailed description on saildrone measurements, OAFlux2 and Argo used in this study.

3. Results

3.1. Dry Air Intrusion

Figure 2 shows daily variations of OAFlux2 wind speed (W), air specific humidity and temperature at 2 m (q_a and T_a), and turbulent heat flux ($Q_{LH} + Q_{SH}$) in the study domain from 27th September to 2nd October 2022. This period corresponds to the movement of Hurricane Ian as it progressed through the GOM and the Atlantic. Three saildrone tracks are superimposed as they directly encountered the impacts of the storm. SD-1032 was located in the northeast, SD-1984 in the northwest of the GOM, while SD-1059 was situated along the U.S. Atlantic coast.

The path of Hurricane Ian is visible in the wind speed fields (Figure 2a), characterized by high wind cores exceeding 15 m s^{-1}. The storm crossed over western Cuba on September 27th, then passed through Florida before heading into the Atlantic on September 28th and 29th. It ultimately impacted the South Carolina coast from September 30th to October 1st. One noteworthy event during the storm's passage was the intensification of northeasterly winds in the northern GOM between September 28th and 30th. This intensification was accompanied by a significant influx of dry air (Figure 2b), leading to a major drop in q_a. During the 3 days, q_a decreased by nearly 50%, from 18 to 19 g/kg to below 9 g/kg. The dry air was also colder, causing T_a to decrease by 3–4°C (Figure 2c). The dry, cold air outbreak was also observed along the U.S. Atlantic coasts, extending into the mid-Atlantic region, in alignment with the eastward progression of mid-latitude high-pressure systems (Figure S1 in Supporting Information S1).

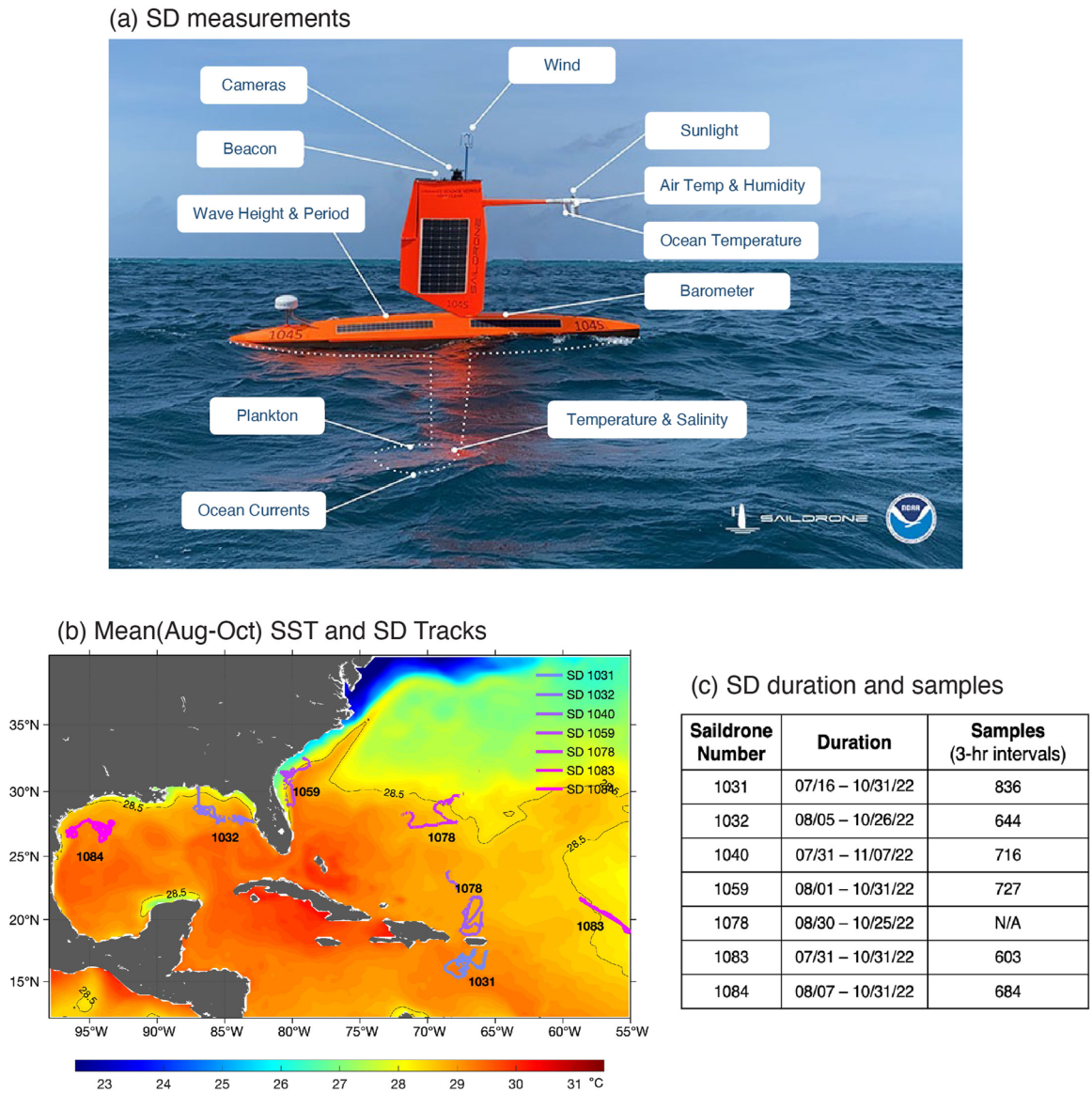

Saildrone Number	Duration	Samples (3-hr intervals)
1031	07/16 – 10/31/22	836
1032	08/05 – 10/26/22	644
1040	07/31 – 11/07/22	716
1059	08/01 – 10/31/22	727
1078	08/30 – 10/25/22	N/A
1083	07/31 – 10/31/22	603
1084	08/07 – 10/31/22	684

Figure 1. (a) Saildrone designed for hurricane missions (source: https://www.pmel.noaa.gov/saildrone-hurricane). (b) OAFlux2 mean SST from 1st August to 31 October 2022, with the seven 2022 saildrone tracks superimposed. The 28.5°C isotherm is marked in black. (c) Key features of the seven saildrones.

The dry cold air over warm, humid sea surface, combined with strong winds, intensified the turbulent transfer of heat (Q_{LH} + Q_{SH}) from the ocean to the atmosphere, reaching above 850Wm^{-2} near Louisiana's coast on September 29th (Figure 2d). This event spanned from the northern Gulf of Mexico to the U.S. mid-Atlantic, increasing turbulent heat fluxes across these areas. The heat fluxes from this dry air outbreak rivaled or surpassed that from Hurricane Ian. The peak of this extreme ocean heat loss in the GOM was on September 29th and 30th (Figure 2d), aligning with the strongest northerly winds (Figure 2a). As winds weakened, the heat fluxes also decreased, despite the continued presence of cold, dry air. More details can be found in Supporting Information S1 (Figure S3).

Cold, dry air with strong northerly winds frequently occur in the GOM, differing in intensity, frequency, and southward penetration (DiMego et al., 1976; Zavala-Hidalgo et al., 2014). While rare in summer, they are common in fall-winter, with a distinct seasonal transition in late September. Not every front crosses the entire GOM; many are confined to the northern region (DiMego et al., 1976). Significant heat fluxes can arise from certain events, as observed by Nowlin and Parker (1974) and Villanueva et al. (2010). The dry air event with Hurricane Ian affected the whole basin for 5 days, highlighting the extraordinary intensity of the dry air originating from

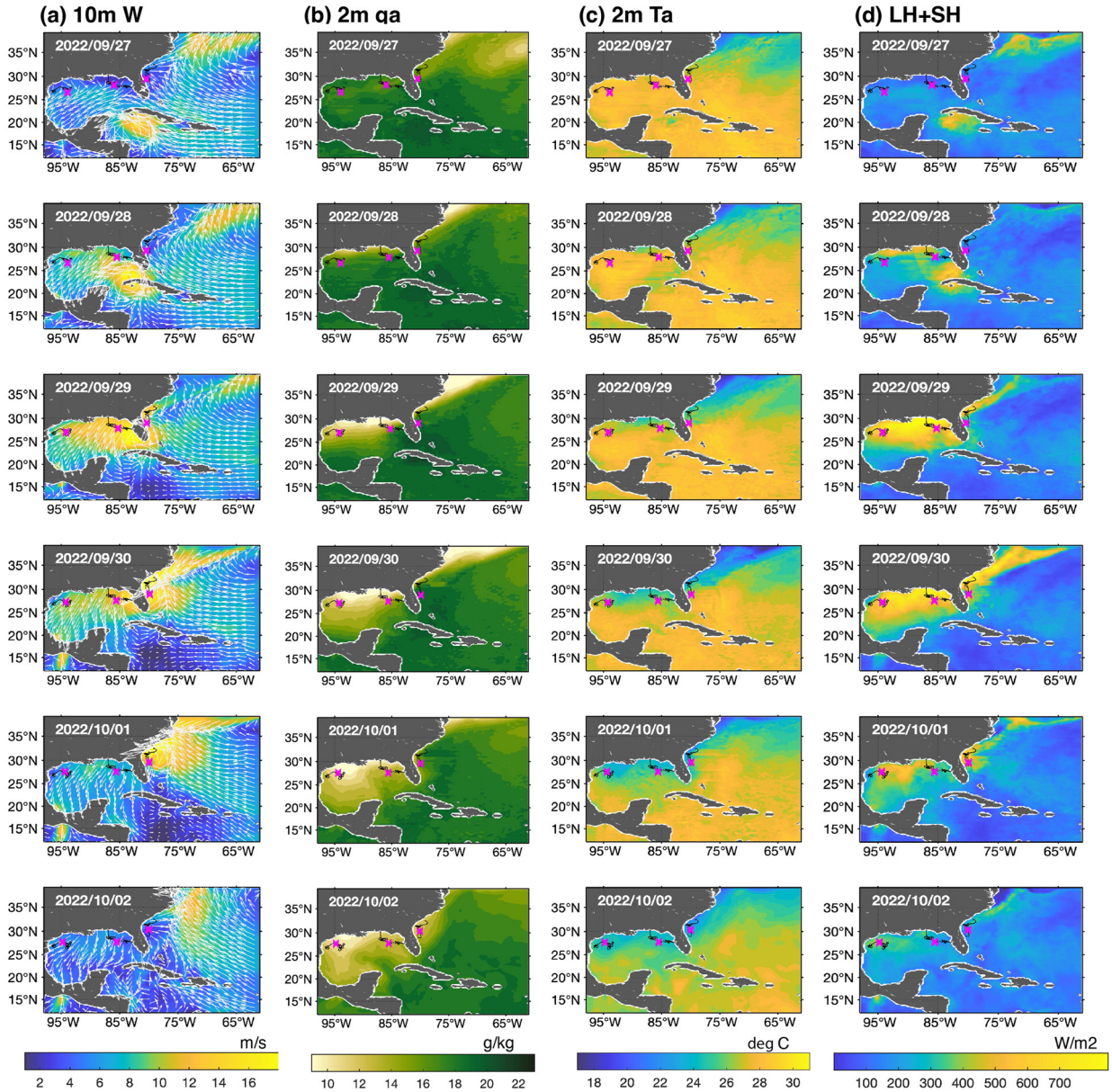

Figure 2. Five-day progression (27th September–2nd October 2022) of air-sea variables: (a) W, (b) q_a, (c) T_a, and (d) $Q_{LH} + Q_{SH}$. Each variable has its own column with daily changes from top to bottom. Tracks of saildrones SD-1032 (northeast), SD-1984 (northwest GOM), and SD-1059 (U.S. Atlantic coast) are superimposed, with midday positions marked by magenta stars.

the drought-stricken mid-latitudes and the strong winds resulting from the convergence of two extreme pressure systems.

3.2. Significant Turbulent Heat Fluxes

Figures 3a–3c depicts the comparison of OAFlux2 and saildrone time series, including W (top panels), q_a (upper middle panels), T_a (lower middle panels), and $Q_{LH} + Q_{SH}$ (bottom panels) along three saildrone tracks. The data span from August 1st to October 31st, with the overlapping period of Hurricane Ian and the dry-air outbreak (September 27th to October 2nd) highlighted in green. During this period, SD-1032 was located northwest of the storm, SD-1059 tracked the eyewall entering the Atlantic, and SD-1084, although off the storm's path, recorded strong air-sea flux variability due to the dry air outbreak. However, there is a notable discrepancy with SD-1059 after September 29th (Figure 3c), where OAFlux2's q_a indicates drier conditions. The humidity sensor on SD1059

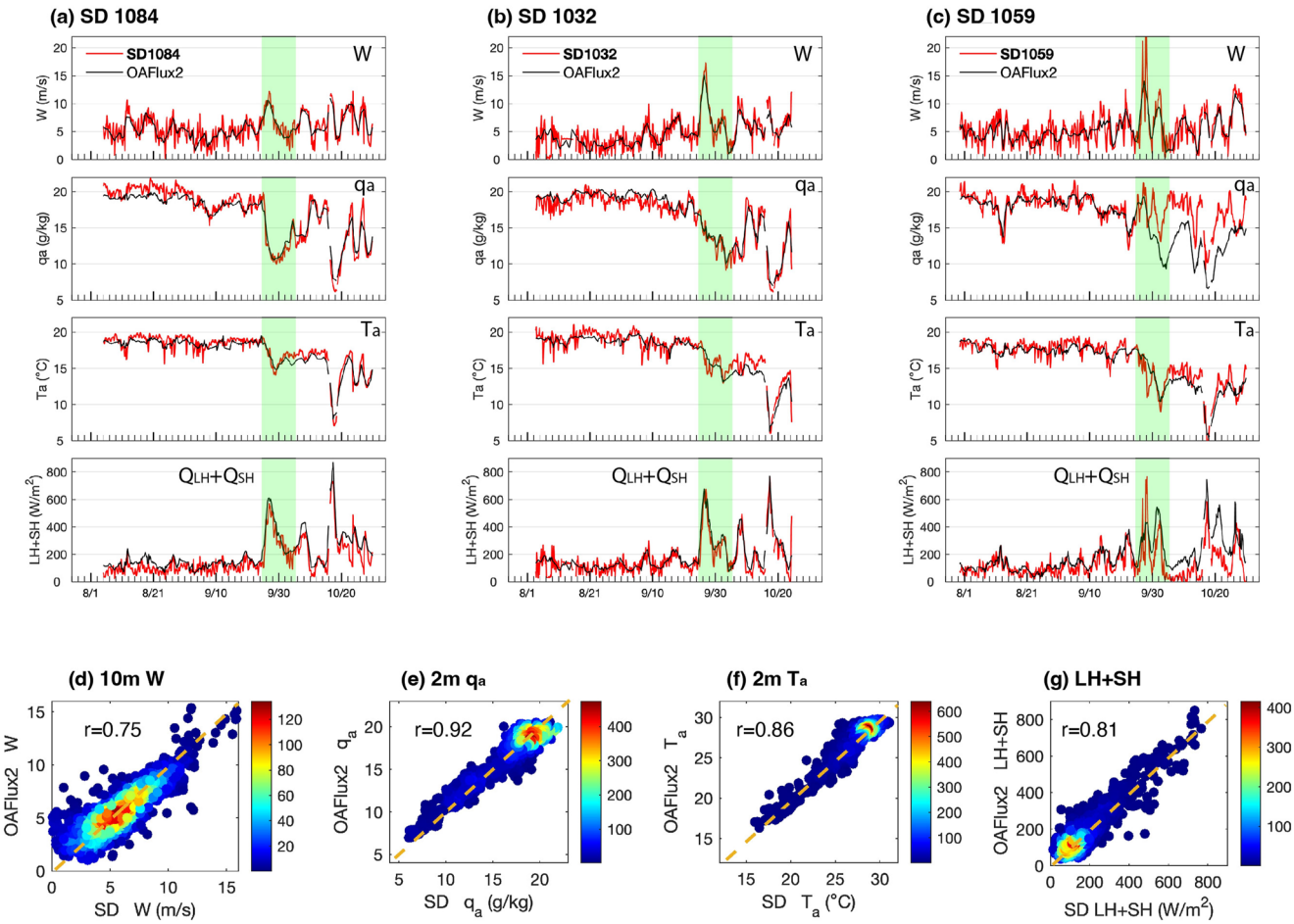

Figure 3. Time series comparison of OAFlux2 with the three saildrones: (a) SD-1084, (b) SD-1032, and (c) SD-1059 span August–October. The semi-transparent green shading denotes the overlapping period of Hurricane Ian and the dry air outbreak. Variables, in order, from top to bottom, are W, q_a, T_a, and $Q_{LH} + Q_{SH}$. The density scatter plots compare OAFlux2 (y-axis) to saildrone (x-axis) for (d) W, (e) q_a, (f) T_a, and (g) $Q_{LH} + Q_{SH}$, with correlation coefficients listed in each scatter plot panel. The dashed straight line represents a linear relationship, and the color denotes the density of data points.

sustained damage around 0500 UTC on September 29th due to the hurricane. This seems to have impacted the mean more than the variability.

Figures 3d–3g shows scatter plots comparing OAFlux2 data with saildrone measurements from all tracks. These comparisons show a high level of agreement, with correlation values ranging from 0.75 to 0.92. The highest correlation is from q_a, while the lowest is from W. These correlation values are statistically significant at the 95% confidence level.

OAFlux2 W adequately captures daily fluctuations along the saildrone paths, but has a limited representation of subdaily variability. The scatter plot of W (Figure 3d) shows generally good agreement between the two sets of winds, despite their derivation from two different observing methods. Discrepancies are observed at low (<5 ms^{-1}) and higher (>12 ms^{-1}) wind speed ranges, with OAFlux2 tending to overestimate at low wind speeds and underestimate at higher wind speeds. During the high wind event associated with the passing of Hurricane Ian and dry air outbreak, OAFlux2 peak winds are weaker by 10%–20% (1–3 ms^{-1}) compared to saildrone peak winds on the 3-hourly basis. This discrepancy exceeds the uncertainty estimate derived from buoy measurements.

Satellites provide area-averaged values of instantaneously measured winds over their spatial footprint, revisiting the same area roughly every 12 hr. Consequently, they are unable to capture the high-frequency details of synoptic wind variability that saildrones, with their 5-min sampling intervals, can capture. Before the advent of autonomous saildrones, measurements in high-wind conditions were somewhat limited. Existing satellite wind retrieval algorithms might not have been fine-tuned for high-wind scenarios. Discrepancies between satellite and in situ

measurements at high winds have been reported (Wright et al., 2021). Evidently, the data from saildrones offer an indispensable complement to satellite-based observations.

OAFlux2 T_a shows a slight cold bias, possibly due to the effect of different sampling methods on measuring moisture gradients during the cold front's eastward shift (Figure S1 in Supporting Information S1). The saildrone travels at 1–3 knots (1.85–5.6 km/hr), producing time-averaged data. SD-1059's path paralleled the front, yielding consistent measurements across 17 km in 3 hr. Conversely, OAFlux2 offers daily satellite data across a more expansive 25 km × 25 km area, capturing broader gradients and varied environments.

Over 3-months, $Q_{LH} + Q_{SH}$ (the bottom panel in Figures 3a–3c) was subdued from August to mid September, averaging around 95Wm^{-2} in the Gulf (SD-1032 and 1084) and about 110 Wm^{-2} on the U.S. Atlantic coast (SD-1059). Q_{SH} contributed 5%–7% of this (Figure S3 in Supporting Information S1). From September 27th to October 2nd, fluxes peaked at 675 Wm^{-2} for SD-1032, 764 Wm^{-2} for SD-1059, and 580 Wm^{-2} for SD-1084. All three saildrones captured the sharp increase in W and the substantial decrease in q_a and T_a. Another major heat loss event was observed around October 16th–18th. These recurrent dry air outbreak events seem to be typical in the fall-winter seasons (DiMego et al., 1976; Zavala-Hidalgo et al., 2014).

An essential question is whether the significant heat fluxes results from Hurricane Ian or a dry air outbreak. Surface air from the storm was humid, contrasting with the dry air mass (Figure 2b). SD-1059 showed a fluctuating q_a pattern from September 27th to October 1st (Figure 3c). Notably, SD-1059's humidity sensor was damaged around September 29th, affecting its mean more than the variability. SD-1059 tracked an area affected by dry air from September 27th (Figure 3b). Humidity rose with Hurricane Ian's arrival on September 29th, then dropped on October 1st as dry air resumed post-storm. Wind speed peaked twice: during the storm and the subsequent cold front, causing spikes in $Q_{LH} + Q_{SH}$ (Figure 3c). It should be noted that the saildrones were not located at the center of the dry air outbreak (Figure 2). According to OAFlux2, the most significant heat loss was near the coasts. The daily mean $Q_{LH} + Q_{SH}$ surpassed 850 Wm^{-2} off the Louisiana coast on September 29th outdoing the heat fluxes induced by Hurricane Ian, which peaked at 650 Wm^{-2}.

3.3. Surface Cooling and Mixed-Layer Deepening

The impact of the significant surface heat loss on subsurface temperature and salinity is examined using Argo data from the GOM between September 10th and 20 October 2022. Figure 4a displays 114 profiles from this period. The profiles, with six or more cycles, were selected for depicting the evolution of density and temperature (Figures 4b and 4c) and are color-coded according to their respective dates. The mixed layer depth (MLD) deepened from about 5 to 40 m from September 27th to 28th, hitting 60 m by October 3rd, with ML temperatures dropping by over 1°C. The MLD changes can arise from wind stirring, vertical entrainment at the ML base, and surface heat loss (Niiler & Kraus, 1977). To examine whether surface heat fluxes alone could explain the observed changes in SST, we conducted the following calculation, assuming that $Q_{LH} + Q_{SH}$ is the primary driver of the change in net heat flux Q_{net},

$$T' = \frac{Q'_{NET}}{\rho c_p h}\Delta t = \frac{(590-95)\,\mathrm{W/m^2}}{1020\,(\mathrm{kg/m^3}) \times 3850\,(\mathrm{J/kg°C}) \times 40\,(\mathrm{m})} \times 5 \times 24 \times 3600(\mathrm{s}) \approx 1.4(°\mathrm{C}) \quad (1)$$

where the prime denotes the change over the $\Delta t = 5$-day period and h is the MLD. Using SD-1084's data, the estimated 1.4°C drop in the MLD temperature, T, matches Argo observations and aligns with the 5-day SST changes from OAFlux2 (Figure 4d). Note that the most notable cooling, ~3°C, was off the Louisiana coast, particularly in the shallow shelf affected by the intense dry air intrusion, where $Q_{LH} + Q_{SH}$ were largest.

3.4. Relative Contribution of q_a and W to Surface Heat Fluxes

Within the study area, Q_{LH} predominantly responds to the dry air outbreak, largely due to the influences of q_a and W (Figures S3 and S4 in Supporting Information S1). To assess their contributions to Q_{LH} variation, we decomposed these variables into mean and anomalous parts (Alexander & Scott, 1997; Cayan, 1992) and rewrite Equation S1 in Supporting Information S1 as follows:

$$Q'_{LH} = \rho_a L_e c_e \left[\overline{W}\Delta q' + W'\overline{\Delta q} + \left(W'\Delta q' - \overline{W'\Delta q'}\right)\right] \quad (2)$$

where the overbars denote time mean over the 3-month period and primes are 3-hr deviations from the mean. The equation can be divided into three components: humidity (Qterm), wind (Wterm), and their covariance (Cterm).

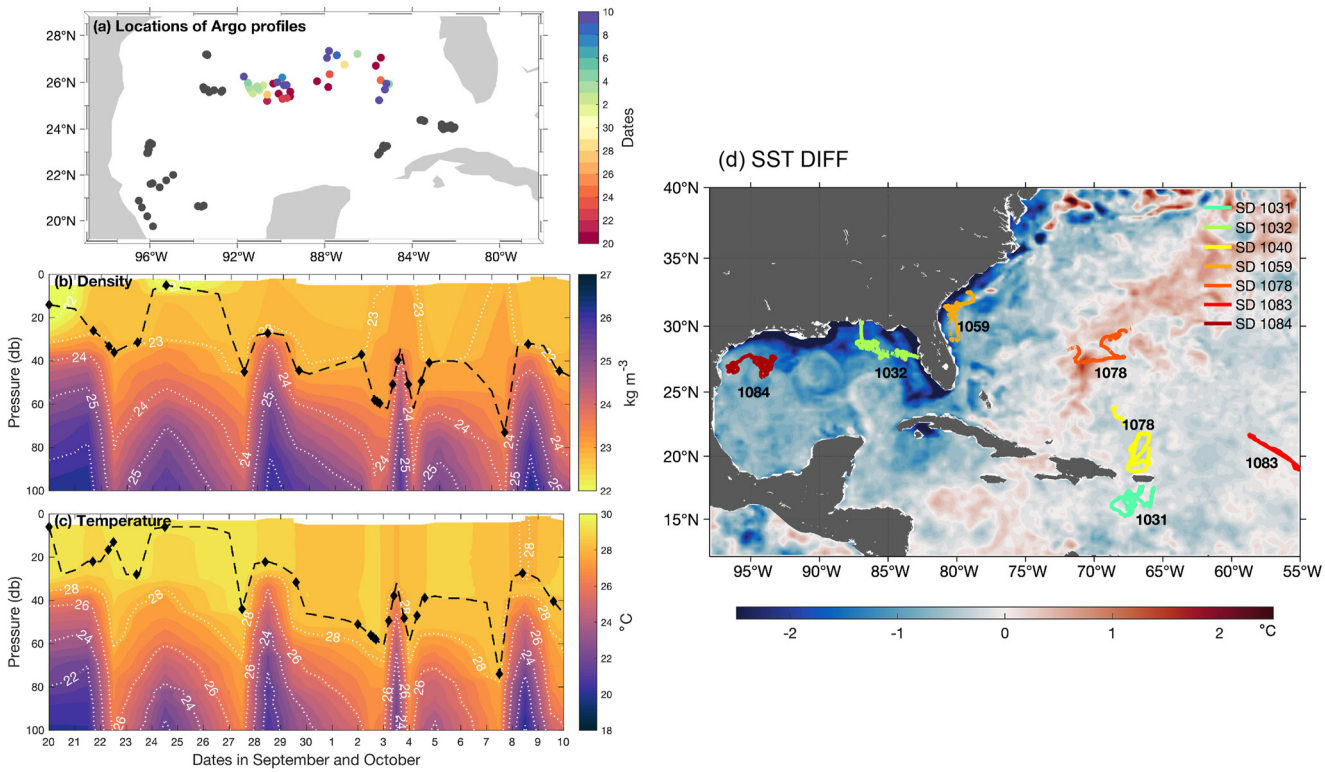

Figure 4. (a) Map of Argo profiles from 20th September to 10th October 2022, with profiles used in this study in color-coded according to their respective dates. (b) Density and (c) temperature structures in the upper 100 m. Dashed black lines in (b) mark the MLD by a density increase of 0.3 kg m^{-3}, and in (c) by a 0.05°C temperature drop from the surface. Argo float availability dates are marked with diamond squares on the MLD lines. (d) The SST difference between October 10th and September 20th using OAFlux2, with the seven saildrone tracks superimposed.

In Figures 5a and 5b, these terms are depicted along the saildrone tracks using c_e and L_e estimated from COARE 3.6. Each panel also displays the contribution of each term to Q'_{LH}, as determined by variance contribution (Γ), calculated using the following expression:

$$\Gamma = {}^{\mathrm{cov}(\mathrm{term},\, Q'_{\mathrm{LH}})}\!/_{\mathrm{var}(Q'_{\mathrm{LH}})} \tag{3}$$

Γ reflects the proportion of variance in Q'_{LH} that can be explained by the respective term under study.

Figures 5a–5c shows that the covariance term, Cterm, is minor with Γ (Cterm) below 0.15. Qterm is more prominent in northwest GOM (SD-1084), while Wterm leads in northeast GOM (SD-1032) and western tropical Atlantic (SD-1059), where Γ (Wterm) surpasses 0.5. During the dry air outbreak, Wterm largely influenced Q'_{LH} values in SD-1032 and SD-1059 regions, while impact of dry air was mainly seen in northwest GOM (SD-1084).

For spatial insight, we mapped Γ values for each term from Equation 3 using OAFlux2 for the 3 months: August–October 2022. Figure 5d shows the Q'_{LH} variance, ranging from 30 to 70 Wm^{-2} in the warm pool region. This range, though significant, is relatively modest compared to the variability associated with the Gulf Stream. Hurricane Ian and the dry air outbreak had a major impact on air-sea heat exchanges in the region. The three corresponding Γ maps (Figures 5e–5g) indicate that Wterm is dominant, with Γ (Wterm) over 0.7 across broad areas in the western tropical Atlantic and Caribbean. Here, Γ (Qterm) is slightly negative, indicating that an increase in Δq reduces the total variance of Q_{LH}. West of GOM and above 30°N latitude, the influence of Wterm diminishes, with Qterm becoming significant. In the areas tracked by saildrones, Γ (Wterm) was either on par with or slightly exceeded Γ (Qterm).

4. Summary and Conclusions

This study investigated an exceptional dry air outbreak in the GOM in late September 2022, triggered by Hurricane Ian and magnified by dry air originating from drought-stricken mid-latitudes, a condition sustained by a persistent high-pressure system. The interaction of dry, cool air with a humid and warm sea surface, together with

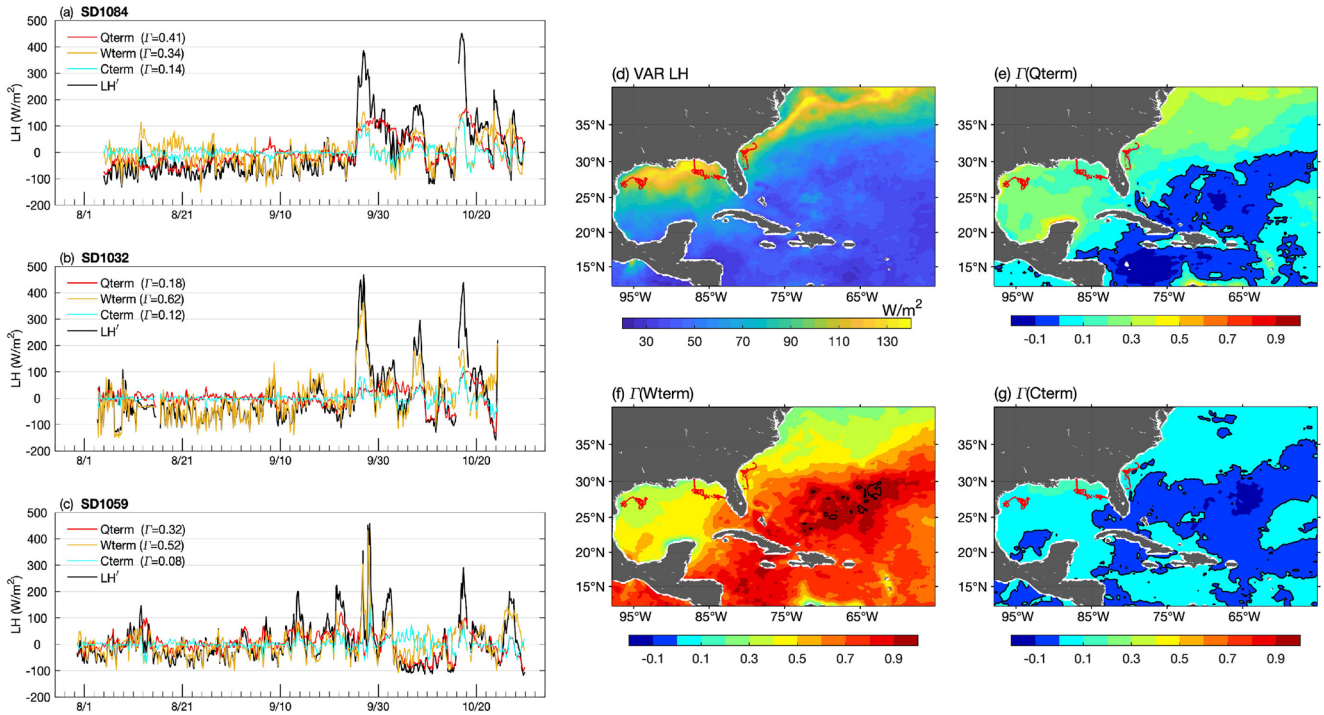

Figure 5. Saildrone Q_{LH} variability from (a) SD 1084, (b) SD 1032, and (c) SD 1059. Q_{LH} is in black, with effects of humidity, wind speed, and covariance in red, tan, and cyan. Variance fraction, Γ, for each term is in the legends. Panels (d)–(g) use OAFlux2 daily means from August to October 2022, presenting (d) Q_{LH} standard deviation and variance contribution of (e) humidity, (f) wind, and (g) covariance. Negative values in (e) and (g) have black contours.

forceful winds, intensified air-sea heat exchanges, leading to significant oceanic heat loss. The 2022 Atlantic hurricane Saildrone mission and satellite data showed turbulent heat fluxes exceeding 850 Wm^{-2}, comparable to the hurricane's direct impacts. Argo float measurements recorded a 40-m deepening of the mixed layer and a 1.4°C temperature drop. The outbreak, concurrent with Hurricane Ian, persisted in the region for over 5 days, highlighting the influence of dry air from drought-affected regions and the forceful winds resulting from the conjunction of two distinct pressure systems.

Saildrone data from northwest GOM (SD-1084) showed significant effects of both wind and humidity on surface heat flux variability. However, in northeast GOM (SD-1032) and the western tropical Atlantic (SD-1059), wind was the main driver of these fluxes. Satellite data from the 2022 Atlantic hurricane season (August–October) corroborated this observation, indicating winds as the dominant factor affecting heat fluxes in the western tropical Atlantic warm pool area. Meanwhile, in regions north and northwest of the warm pool, both humidity and wind significantly impacted the fluxes. These insights underline the complex relationship between dynamic and thermodynamic factors in shaping turbulent heat fluxes in the western tropical Atlantic. Understanding this balance is essential for gaining insights into tropical air-sea interactions and improving the prediction skills of the intensity and trajectory of tropical storms.

The study also found that saildrones, equipped with 5-min high-frequency sampling capability, offer detailed views on wind variability during weather events like hurricanes and dry air outbreaks. These details are often missed by satellites due to averaging over sensor's footprint and 12-hr gaps between revisits. When comparing on a 3-hourly basis, saildrone peak winds exceed OAFlux2 peak winds by 10%–20%. Clearly, saildrones serve as invaluable complement to satellite wind measurements.

Our study concluded that the simultaneous impact of hurricane and dry air outbreak led to a significant reduction in the heat content of the upper ocean in the Gulf. Interestingly, water temperatures remained below their pre-outbreak levels for as long as 10 days after the event (Figure 4). Considering that tropical cyclones rely on warm waters for energy and intensification, this extended period of heat content recuperation is significant for modeling and predicting cyclone activities in this area.

Data Availability Statement

The NOAA saildrone hurricane observations are described in Foltz et al. (2022) and Zhang et al. (2023). Argo profiles were downloaded from Coriolis Global Data Acquisition Center (Argo, 2000). The OAFlux2 data sets are currently being archived for online release (Yu & Weller, 2007) and the subsets associated with this study are available from Figshare data repository (Yu, 2023).

Acknowledgments
LY is sincerely grateful for funding support for this study from NASA Ocean Vector Wind Science Team (OVWST) program, Grant 80NSSC23K0981, NASA Making Earth System Data Records for Use in Research Environments (MEaSUREs) Program, Grant 80NSSC18M0079, and NOAA Ocean Monitoring and Observing (GOMO) program, Grant NA19OAR4320074. This is PMEL contribution #5547. We thank the two anonymous reviewers for their constructive comments.

References

Alexander, M. A., & Scott, J. D. (1997). Surface flux variability over the North Pacific and North Atlantic oceans. *Journal of Climate*, *10*(11), 2963–2978. https://doi.org/10.1175/1520-0442(1997)010<2963:SFVOTN>2.0.CO;2

Argo. (2000). Argo float data and metadata from Global Data Assembly Centre (Argo GDAC). *SEANOE*. https://doi.org/10.17882/42182

Bucci, L., Alaka, L., Hagen, A., Delgao, S., & Beven, J. (2023). *Tropical cyclone report: Hurricane Ian*. National Hurricane Center, NOAA National Weather Service. Retrieved from https://www.nhc.noaa.gov/data/tcr/AL092022_Ian.pdf

Cayan, D. R. (1992). Variability of latent and sensible heat fluxes estimated using bulk formulae. *Atmosphere-Ocean*, *30*, 1–42. https://doi.org/10.1080/07055900.1992.9649429

DiMego, G. J., Nosart, L. F., & Endersen, G. W. (1976). An examination of the frequency and mean conditions surrounding frontal incursions into the Gulf of Mexico and Caribbean Sea. *Monthly Weather Review*, *104*(6), 709–718. https://doi.org/10.1175/1520-0493(1976)104<0709:aeotfa>2.0.co;2

Fairall, C. W., Bradley, E. F., Hare, J. E., Grachev, A. A., & Edson, J. B. (2003). Bulk parameterization of air–sea fluxes: Updates and verification for the COARE algorithm. *Journal of Climate*, *16*(4), 571–591. https://doi.org/10.1175/1520-0442(2003)016,0571:BPOASF.2.0.CO;2

Foltz, G. R., Zhang, C., Meinig, C., Zhang, J. A., & Zhang, D. (2022). An unprecedented view inside a hurricane. *Eos*, *103*. https://doi.org/10.1029/2022EO220228

Nagano, A., & Ando, K. (2020). Saildrone-observed atmospheric boundary layer response to winter mesoscale warm spot along the Kuroshio south of Japan. *Progress in Earth and Planetary Science*, *7*(1), 43. https://doi.org/10.1186/s40645-020-00358-8

Niiler, P. P., & Kraus, E. B. (1977). One-dimensional models of the upper ocean. In E. B. Kraus (Ed.), *Modelling and prediction of the upper layers of the ocean* (Vol. 143–172).

Nowlin, W. D., Jr., & Parker, C. A. (1974). Effects of a cold-air outbreak on shelf waters of the Gulf of Mexico. *Journal of Physical Oceanography*, *4*(3), 467–486. https://doi.org/10.1175/1520-0485(1974)004<0467:eoacao>2.0.co;2

Tilinina, N., Gavrikov, A., & Gulev, S. K. (2018). Association of the North Atlantic surface turbulent heat fluxes with midlatitude cyclones. *Monthly Weather Review*, *146*(11), 3691–3715. https://doi.org/10.1175/MWR-D-17-0291.1

Villanueva, E. E., Mendoza, V. M., & Adem, J. (2010). Sea surface temperature and mixed layer depth changes due to cold-air outbreak in the Gulf of Mexico. *Atmósfera*, *23*, 325–346.

Wang, C., Lee, S.-K., & Enfield, D. B. (2008). Atlantic warm pool acting as a link between Atlantic multidecadal oscillation and Atlantic tropical cyclone activity. *Geochemistry, Geophysics, Geosystems*, *9*(5), Q05V03. https://doi.org/10.1029/2007GC001809

Wright, E. E., Bourassa, M. A., Stoffelen, A., & Bidlot, J.-R. (2021). Characterizing buoy wind speed error in high winds and varying sea state with ASCAT and ERA5. *Remote Sensing*, *13*(22), 4558. https://doi.org/10.3390/rs13224558

Yoneyama, K., & Parsons, D. B. (1999). A proposed mechanism for the intrusion of dry air into the tropical western Pacific region. *Journal of the Atmospheric Sciences*, *56*(11), 1524–1546. https://doi.org/10.1175/1520-0469(1999)056<1524:APMFTI>2.0.CO;2

Yu, L. (2023). OAFlux2_NATL_2022.nc [Dataset]. figshare. https://doi.org/10.6084/m9.figshare.23909532.v1

Yu, L., & Weller, R. A. (2007). Objectively analyzed air–sea heat fluxes for the global ice-free oceans (1981–2005). *Bulletin America Meteorology Social*, *88*(4), 527–540. https://doi.org/10.1175/BAMS-88-4-527

Zavala-Hidalgo, J., Romero-Centeno, R., Mateos-Jasso, A., Morey, S. L., & Martínez-López, B. (2014). The response of the Gulf of Mexico to wind and heat flux forcing: What has been learned in recent years? *Atmósfera*, *27*(3), 317–334. https://doi.org/10.1016/s0187-6236(14)71119-1

Zhang, C., Foltz, G. R., Chiodi, A., Mordy, C., Edwards, C., Meinig, C., et al. (2023). Hurricane observations by uncrewed systems. *Bulletin America Meteorology Social*, *104*(10), E1893–E1917. https://doi.org/10.1175/BAMS-D-21-0327.1

References From the Supporting Information

Edson, J. B., Jampana, V., Weller, R. A., Bigorre, S., Plueddemann, A. J., Fairall, C. W., et al. (2013). On the exchange of momentum over the open ocean. *Journal of Physical Oceanography*, *43*(8), 1589–1610. https://doi.org/10.1175/JPO-D-12-0173.1

Fairall, C. W., Bradley, E. F., Rogers, D. P., Edson, J. B., & Young, G. S. (1996). Bulk parameterization of air–sea fluxes for TropicalOcean–GlobalAtmosphereCoupledOcean–atmosphere response experiment. *Journal of Geophysical Research*, *101*(C2), 3747–3764. https://doi.org/10.1029/95JC03205

Liu, W. T., Katsaros, K. B., & Businger, J. A. (1979). Bulk parameterization of air-sea exchanges of heat and water vapor including the molecular constraints at the interface. *Journal of the Atmospheric Sciences*, *36*(9), 1722–1735. https://doi.org/10.1175/1520-0469(1979)036<1722:BPOASE>2.0.CO;2

Meinig, C., Burger, E. F., Cohen, N., Cokelet, E. D., Cronin, M. F., Cross, J. N., et al. (2019). Public-private partnerships to advance regional ocean-observing capabilities: A saildrone and NOAA-PMEL case study and future considerations to expand to global scale observing. *Frontiers in Marine Science*, *6*, 448. https://doi.org/10.3389/fmars.2019.00448

Shepard, D. (1968). A two-dimensional interpolation function for irregularly-spaced data. *Proceedings of the 1968 23rd ACM National Conference (ACM '68)* (Vol. 23, pp. 517–524).

UK Met Office. (2005). OSTIA L4 SST analysis. Version 1.0. PO.DAAC, https://doi.org/10.5067/GHOST-4FK01

Yu, L. (2021). Emerging pattern of wind change over the Eurasian Marginal Seas revealed by three decades of satellite ocean-surface wind observations. Special issue "Remote sensing of air-sea fluxes". *Remote Sensing*, *13*(9), 1707. https://doi.org/10.3390/rs13091707

Yu, L., & Jin, X. (2014). Insights on the OAFlux ocean surface vector wind analysis merged from scatterometers and passive microwave radiometers (1987 onward). *Journal of Geophysical Research: Oceans*, *119*(8), 5244–5269. https://doi.org/10.1002/2013JC009648

Yu, L., & Jin, X. (2018). A regime-dependent retrieval algorithm for near-surface air temperature and specific humidity from multi-microwave sensors. *Remote Sensing of Environment*, *215*, 199–216. https://doi.org/10.1016/j.rse.2018.06.001

Zhang, D., Cronin, M. F., Meinig, C., Farrar, J. T., Jenkins, R., Peacock, D., et al. (2019). Comparing air-sea flux measurements from a new unmanned surface vehicle and proven platforms during the SPURS-2 field campaign. *Oceanography*, *32*(2), 122–133. https://doi.org/10.5670/oceanog.2019.220